Effect of graphene residual carbon content on electrochemical properties of NiS/GR composites

Fang Yang[1],*, Hao Huang[1] , and Wei Dong[1]

[1] *College of Material Science and Engineering, Liaoning Technical University, Fuxin 123000, Liaoning, China*

ABSTRACT

Graphene plays an essential role in the energy conversion field because of its particular geometrical structures. With its development, the study of its by-products (e.g., graphene residual carbon) is urgent. Herein, the novel synthesis of nickel sulfide and carbon-based material composite (NiS/GR) by one-step hydrothermal method via utilization of graphene residual carbon prepared by Hummer method as carbon-based material. The influence of graphene residual carbon content (5%, 10%, and 15%) on the electrochemical performance of NiS/GR in investigated. It is that when the content of graphene residual carbon is 5%, exhibiting the highest specific capacitance (774 F/g at 1 A/g), good rate capability (78.1% retention after current density increases to 10 A/g) and good cycling performance (77.2% capacitance retention after 1000 cycles at 5 A/g).

1 Introduction

In the past decade, more and more nature issues have received increasing attention, such as climate change, species extinction, sea-level rise, and so on, which owned to the gradual increase in the greenhouse effect and the depletion of fossil fuels [1]. A clean, safe, efficient, and convenient energy alternative to fossil fuels is urgently needed [2, 3]. Recently, converting clean and renewable resources such as solar energy, wind energy, and tidal energy into electric energy has become increasingly popular. The rapid development of electric energy storage devices provides a convenient, efficient way for storing and conversing electrochemical energy [4, 5]. Supercapacitors have drawn much attention, owned to their fast charge and discharge rates, long-term cyclability, and balance of energy density and power density have outstanding performance among electrochemical energy storage devices [6, 7]. Supercapacitors rely on two charge storage mechanisms, which are electric double layer capacitance(EDLC) and pseudocapacitance [8]. The difference is that the former adsorb charges at the interface between electrodes and electrolytes, and the latter undergo fast reversible redox reactions between electrode materials and electrolyte ions [9]. Carbon-based materials are the earliest electrode materials used in supercapacitors, and their high conductivity, huge specific surface area, complex pore structure, and stable physical and chemical properties are the main reasons why carbon-based materials are typical representatives of EDLC [10], but it is also widely known that carbon-based electrode materials have varying degrees of

Address correspondence to E-mail: yangf1226@126.com

shortcomings, such as low capacitance, the complex synthesis process, high cost, and low yield of carbon nanotube (CNTs), carbon fiber (CFAs), and thin layer graphene [1, 11].As for transition metal compounds as a typical representative of pseudocapacitance have been regarded as ideal electrode material in the future because of their various valence states, rich natural reserves, and high capacitance performance, but low electrical conductivity of oxides and hydroxides dominated by manganese-based, molybdenum-based, cobalt-based, nickel-based, and other elements lead to good rate performance and cycle performance cannot be obtained [12]. Therefore, the preparation of electrode materials with superior performance, low price, and high conductivity is still a challenge and the future research focus is the performance coordination between carbon-based materials and transition metal compounds.

In recent years, cobalt sulfide, nickel sulfide, and nickel-cobalt-sulfur ternary transition metal sulfides as new electrode materials for electric energy storage have become a hotspot [13–15]. The reason is that sulfur has a lower electronegativity than oxygen, which gives sulfides a more flexible structure, richer redox reactions, and higher electrical conductivity than oxides [16]. Among these metal sulfides, NiS is considered a potential electrode material for supercapacitors, perhaps due to its high theoretical capacity (590 mAh/g), rich redox reaction active sites, low cost, and environmental friendliness [13, 17]. $Ni(OH)_2$ microflowers was utilized by Zhao et al. [16] as a precursor to synthesize NiS microflowers by adjusting the vulcanizing time. This electrode resulted in a high specific capacitance of 1315.4 F/g at 1 A/g. Hu et al. [18] prepared β-NiS microspheres via controlling the hydrothermal reaction time for 3 h with a high specific capacitance of 313.1 mAh/g at 1 A/g. Due to the aggregation between the active materials, the further improvement of the electrochemical property of the single sulfides is difficult, which reduces the utilization rate of the active materials.

What's more significant, conductivity, redox activity, morphology, and structural stability can also affect the electrochemical properties of sulfides [19] but which can be optimized by compositing with carbon-based materials [20]. Wu et al. [21] synthesized hybrid composites consisting of NiS and Zeolitic-imidazolate frameworks derived from porous carbon (ZIFs-C), which displayed 1827 F/g at 1 A/g.

CNFs-NiS electrode was obtained through wrapping carbon nanofibers with NiS by Xu et al. [13], which exhibits high capacitance retention of 88.7% after 5000 cycles at 1 A/g.

With the discovery of many excellent properties, graphene has swiftly become an indispensable means to improve the properties of materials. But during preparing graphene by the modified Hummer's method, will produce about 72% graphene residual carbon (GR). The direct discard of GR will pollute the environment and cause a waste of resources because of its acidic nature. But, the recovery and utilization of these resources are rarely studied. Compared with the pure NiS (537.8 F/g at 1 A/g), the synthesized 5NiS/GR electrode not only shows higher specific capacitance (774 F/g at 1 A/g), but the rate performance (78.1% retention after current density increases to 10 A/g) and the cycle performance (77.2% capacitance retention after 1000 cycles at 5 A/g) have improved when introducing the 5% content of GR into NiS. The enhanced electrochemical behaviors are mainly due to the 5% content of GR in the composite electrode (5%, 10%, and 15%) provides NiS nanomaterials more nucleation sites and proper dispersion of NiS and increases the active specific surface area of its contact with the electrolyte and promotes the reaction.

2 Results and discussion

2.1 Phase and morphology analysis of the sample

Figure 1 demonstrates the XRD patterns of GR, NiS, and three groups of NiS/GR composite (5%, 10%, and 15%). For the GR sample, a broad peak at ∼25° corresponding to the (002) plane of graphite carbon, indicating that GR is amorphous carbon. The detected peaks of NiS sample at 2θ = 18.40°, 30.26°, 32.18°, 35.66°, 37.34°, 40.42°, 48.80°, 50.10°, 52.60°, 56.22°, 57.40°, 59.64°, 72.52°, 75.58°and 79.66° corresponding well to the (110), (101), (300), (021), (220), (211), (131), (410), (401), (321), (330), (012), (312), (042), and (440) planes of NiS (PDF#12-0041), respectively. The XRD profile of three groups of NiS/GR shows detected peaks at 29.98°, 34.48°, 45.67°, 53.23°and 72.70° are indexed to the (100), (101), (102), (110) and (202) faces of NiS (PDF#77-1624), respectively. Further, a broad peak at ∼25° corresponding to graphite carbon can
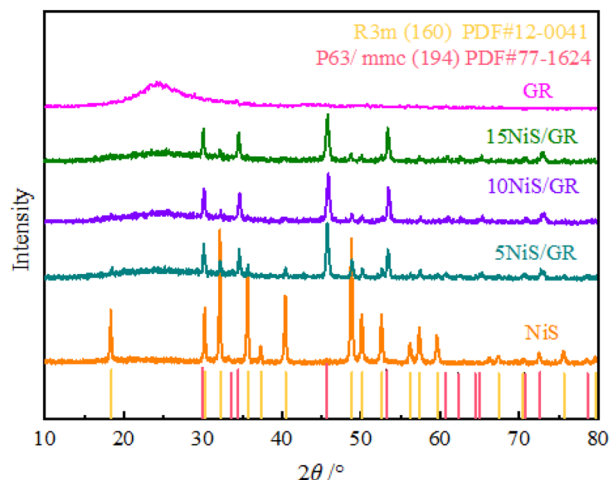
Fig. 1 XRD pattern of GR, NiS, 5NiS/GR, 10NiS/GR, and 15NiS/GR

be proved in the XRD patterns of NiS/GR. The XRD result shows that the addition of GR has a certain effect on the crystal structure of the NiS, which changes the NiS crystal phase from R3m (160) to R3m (160) and P63/ mmc (194) mixed crystal phase. The peak intensity of three groups of NiS/GR composite samples is significantly lower than that of pure NiS, indicating that the introduction of GR decreases the proportion of NiS because of the addition of GR (5%, 10%, and 15%) that reduces the peak intensity of NiS [22, 23].

The morphology of all obtained samples is characterized by SEM. As shown in Fig. 2a, GR shows a folded tulle shape with a rugged surface and a multi-layer morphology. From Fig. 2b, the prepared NiS exhibits a micronflower structure with a diameter of 4 μm, formed by the aggregation of micronrods with a diameter of 2 μm. To compare with the NiS, confirming that the morphology of NiS/GR under introducing GR has changed. From Fig. 2c-e, nano-sphere NiS with a diameter <1 μm and distributed on the GR surface. The SEM indicates that the addition of GR not only transforms the morphology of NiS particles but also reduces its size and makes it distributed. The change of the morphology is equal to the surface-active site, which will affect the contact between the electrode material and the electrolyte, which could bring different influences on the specific capacitance or other electrochemical properties.

The TEM images of NiS/GR in Fig. 3a, b illustrate that black NiS evenly wrapped by the transparent GR, and the diameters ∼200 nm of these NiS nano-spheres. From the HRTEM diagram of NiS/GR in Fig. 3c, lattice fringes on the NiS. The d-spacing of NiS belonging to the (101) plane is 0.26 nm. Additionally, the selected area electron diffraction (SAED) pattern (Fig. 3d) reveals these rings indexed to PDF#12-0041 (yellow) and PDF#77-1624 (red), respectively, indicating the crystalline nature of the NiS/GR electrode, which is accordance with the XRD result.
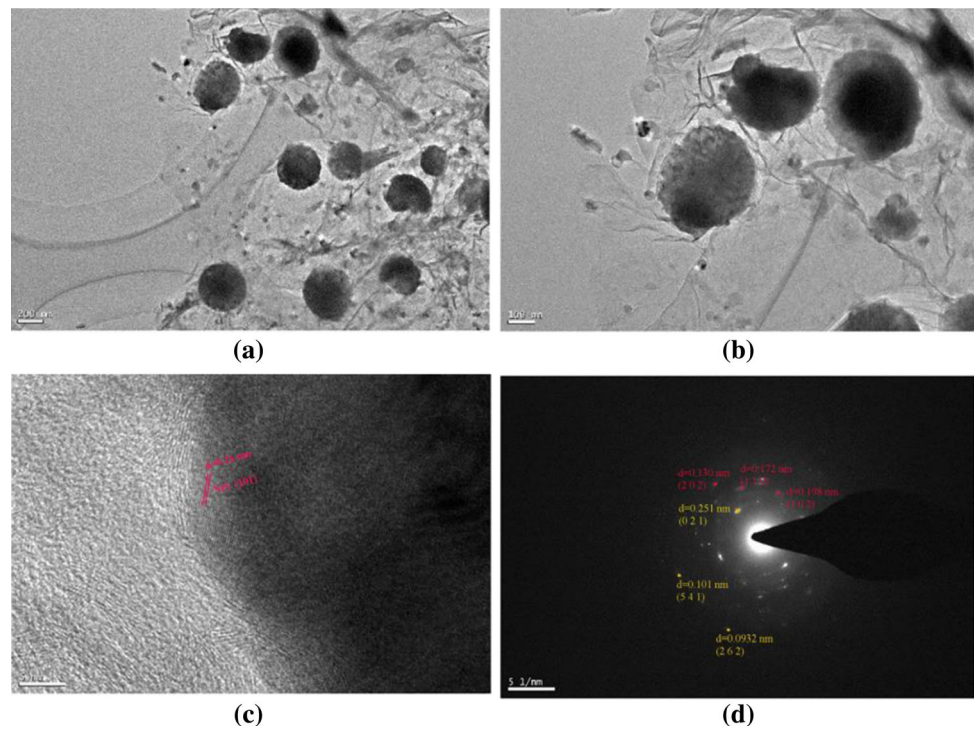
2.2 Electrochemical performance analysis

Galvanostatic charge/discharge (GCD) curves of 5NiS/GR, 10NiS/GR, and 15NiS/GR compared with NiS at a current density of 1 A/g are shown in Fig. 4a. As you can see, the charge/discharge diagrams show a platform in the range of 0.35 to 0.45 V, manifesting the presence of Faradaic reactions of the electrodes, displaying the pseudocapacitance behavior. The discharge time of 5NiS/GR and 10NiS/GR electrode are higher than NiS electrode. It is noteworthy that the discharge time of 5NiS/GR is longer than others. This result shows that the addition of GR has no impact on the pseudocapacitance of NiS in NiS/GR, and can improve the specific capacitance when adding a certain content of GR, which should be associated with the enhancement of electrical conductivity. The calculated specific capacitance is 774 F/g, 724 F/g, 510 F/g, and 537.8 F/g at 1 A/g for 5NiS/GR, 10NiS/GR, 15NiS/GR, and NiS by formula 6, respectively. GCD testing results demonstrate that the importance of a suitable amount of GR can promote the specific capacitance of the electrode, and the excessive addition of GR could decrease the load of NiS on the electrode material [24].

Cyclic voltammetry (CV) curves of all obtained samples are shown in Fig. 4b. Comparing the enclosed CV curve area among these electrodes, which shows 5NiS/GR is the largest, indicating that the specific capacitance of 5NiS/GR is the highest. Furthermore, it can be seen from the image that the presence of reversible redox peaks in the CV curves of NiS and NiS/GR, indicating that the exchange of electron. These redox peaks can be related to the conversion of Ni^{2+} to Ni^{3+}. According to the
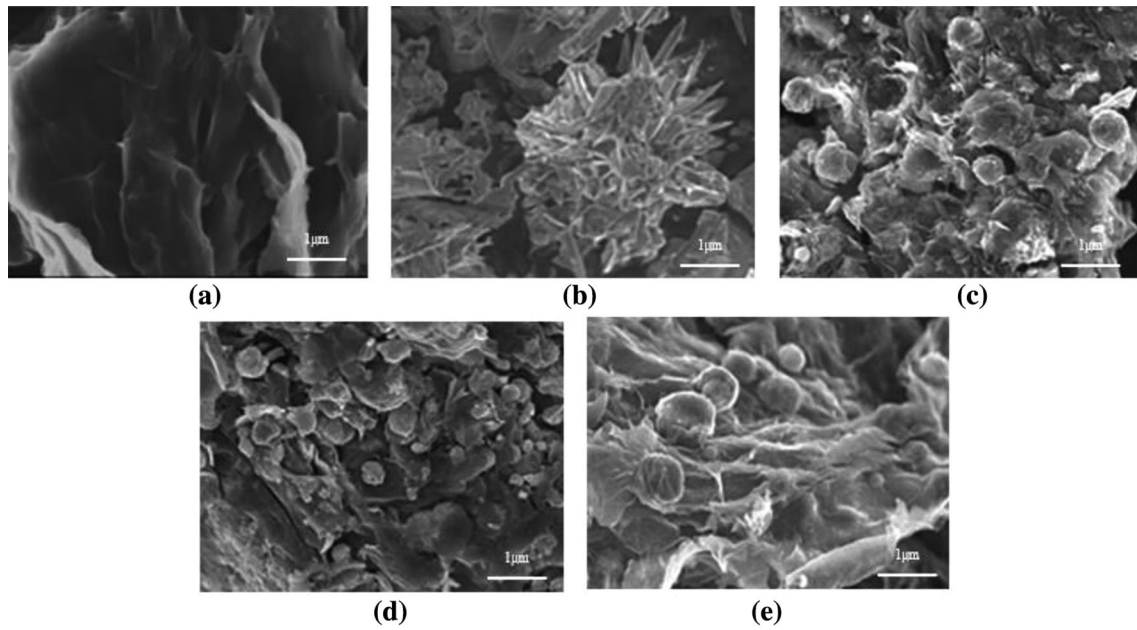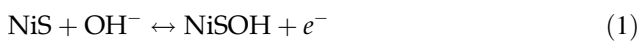
Fig. 2 SEM images of **a** GR, **b** NiS, **c** 5NiS/GR, **d** 10NiS/GR and **e** 15NiS/GR

**Fig. 3** TEM images (**a**, **b** and **c**) and SADE image of NiS/GR

reference [25], it is inferred that the redox reaction occurs in the current peak region as follows.

$$NiS + OH^- \leftrightarrow NiSOH + e^- \tag{1}$$

To further investigate the electrochemical performance of the 5NiS/GR electrode, CV tests are conducted at different low scan rates, as shown in Fig. 4c. Cyclic voltammetry curves maintain almost the same shapes when scan rates increase from 2 to 8 mV/s. Furthermore, the anodic peaks shift to high potential, while cathodic peaks shift towards low potential, as a direct consequence of different scan rates can't match the ion diffusion rate in the electrolyte. With the increase of the scan rate, the
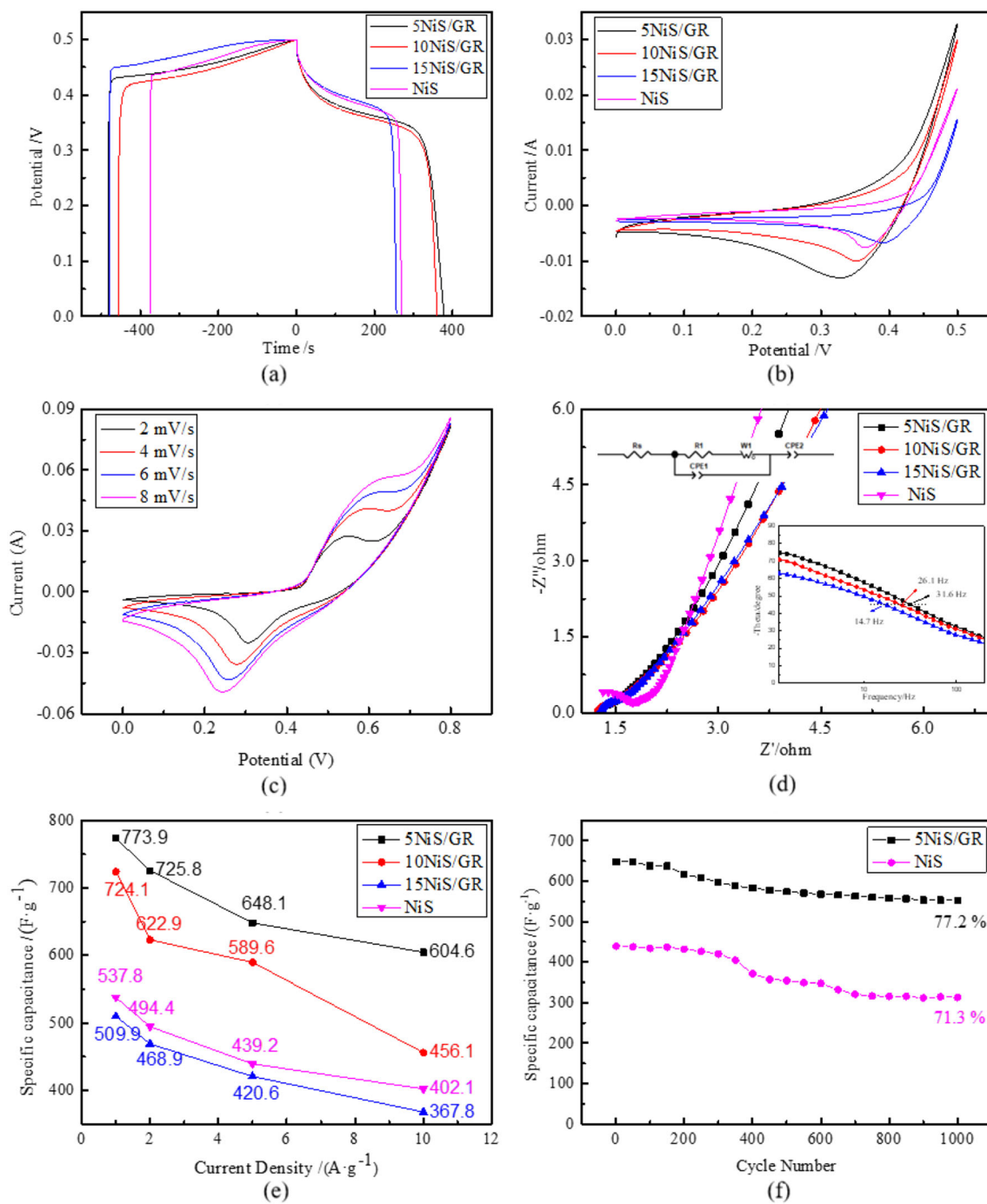
Fig. 4 **a** GCD curve at 1 A /g, **b** CV curve at 20 mV/s, **c** CV curves of 5NiS/GR at different scanning rates, NiS and NiS/GR. **d** Nyquist plots and Bode plots of phase angle versus frequency, **e** Multiplier performance testing, **f** Cycle performance testing

utilization rate of the active material is limited as the redox reaction takes place only at the surface of the electrode material. As a result, the specific capacitance decreases with the increase of the scan rate [26].

The Electrochemical impedance spectroscopy (EIS) study is an important technology to understand the reaction kinetics between electrode and electrolyte, as shown in Fig. 4d. Generally, the Nyquist plot can be divided into two parts, a straight line in the low-frequency and a semicircle in the high-frequency. The

intercept of the semicircle on the real axis in the high-frequency region designates the solution resistance (Rs) of the electrolyte. The diameter of the semicircle corresponds to the charge transfer resistance (Rct) of the electrode material. The slope is associated with the diffusion resistance or the Warburg impedance (W) [27, 28]. The high-frequency incomplete semicircle indicates a large electroactive surface area, high conductivity, and low value of charge transfer resistance [29]. The equivalent circuit model and the fit values are shown in the inset and Table 1, respectively. 5NiS/GR has the lowest Rct value and the fastest electrolyte ion diffusion rate (smaller W-T), indicating that introducing the proper content of GR can improve the conductivity of NiS. Combined with the SEM image, the existence of GR and the good dispersion of NiS increase the active surface area of contact with the electrolyte, which indicates a positive synergistic effect between NiS and GR that leads to superior electrochemical performance. Furthermore, in the Bode plots (inset of Fig. 4d), the characteristic frequency at the phase angle of 45 °of 5NiS/GR, 10NiS/GR, and 15NiS/GR are determined to be 31.6, 26.1, and 14.7 Hz, corresponding to the time constant τ of 0.0316, 0.0383, and 0.0680, respectively. The smaller time constant τ of the 5NiS/GR electrode indicates the ultrafast frequency response, again confirming the efficient charge transport of 5NiS/GR during the charge and discharge process [30].The relationship between specific capacitance and current density (1, 2, 5, and 10 A/g) in Fig. 4e. The rate capability (retention after current density increases to 10 A/g) of NiS, 5NiS/GR, 10NiS/GR, and 15NiS/GR electrodes are 74.7%, 78.1%, 63.0%, and 72.0%, respectively. It may be due to the proper content (5%) of GR improve the rate capability of NiS electrode. The cycling stability of electrodes is a key factor for its practical applications. As shown in Fig. 4f, both NiS and 5NiS/GR exhibit good excellent cycling stabilities, 71.3% and 77.2% of initial specific

capacitances were still retained at the current density of 5 A/g after 1000 cycles, which indicates that 5% content of GR could improve NiS/GR electrode cycling stability. Obviously, in the first 200 cycles, the capacity change of the NiS electrode is similar to the 5NiS/GR electrode, and the specific capacitance of pure NiS attenuates rapidly when the cycles increase to 400. The possible reason for this phenomenon is that active material (NiS) falls off during the cycle, resulting in a decrease in the number of active materials involved in energy storage in the subsequent charge and discharge. It shows that the addition of GR is helpful to improve the cyclic stability of the electrode through immobilizing active materials. The specific capacitance of this work presents well than previous literature on similar nickel sulfides composites (Table 2).

To further explore the kinetic analyses of 5NiS/GR electrodes based on CVs [38]. The charge storage mechanism can be divided into two core processes: capacitive contribution and diffusion-controlled contribution. According to formula 2, the relationship between peak current (i) and scan rates (v) can be described.

The slope of the fit line is calculated by log (v)-log (i) to determine the b values [39]. The b values at various scan rates could reveal the kinetics [40]. Generally, the material mainly stores energy through charge adsorption (capacitive contribution) could be ascribed when the b values are close to 1. While the material energy storage is realized through the intercalation/deintercalation of electrolyte ions in the electrode material (diffusion-controlled contribution), the b values tend to 0.5 [41]. The b value of the 5NiS/GR electrode is 0.52 (as shown in Fig. 5a), which shows that the main form of energy storage is more inclined to diffusion-controlled contribution. In addition, the proportion of capacitive contribution to the total capacitance can be determine quantitatively according to the following formula 3

$$\log i = b \times \log v + \log a \qquad (2)$$

I (V) represents the current response at a fixed position in formula 3, v represents the scanning rate, and $k_1 v$ and $k_2 v^{1/2}$ are associated with the capacitive and diffusion-controlled contribution, respectively [42]. By drawing the fitting lines of I (V)/$v^{1/2}$-$v^{1/2}$ at various potentials, the slope and intercept of the fit lines can be calculated, which correspond to k_1 and k_2, respectively. Using these series of k_1 and k_2 values,

Table 1 Fitting Nyquist values of NiS/GR

	R_s	R_{ct}	W-R	W-T	W-P
5NiS/GR	1.21	0.432	2.74	0.0286	0.355
10NiS/GR	1.18	0.480	3.22	0.0292	0.353
15NiS/GR	1.25	0.509	3.727	0.032	0.430
NiS	0.791	0.801	1.67	0.00140	0.429

Table 2 A comparison table of the capacity of NiS/GR with previous literatures on similar nickel sulfides

Material	Electrolyte	Current density	Specific capacitance (F/g)	References
NiS/PEDOT: PSS-5	2 M KOH	1.11 A/g	722.41	[31]
NiO/NiS	3 M KOH	1 A/g	386.7	[32]
CuS/NiS	1 M KOH	1 A/g	122	[33]
NiS/C-dot	2 M KOH	2 A/g	880	[34]
NiO/NiS@CNT	1 M KOH	1 A/g	809.7	[35]
NiS/rGO	2 M KOH	1 A/g	715.68	[36]
NiS/RGO	1 M KOH	1.1 A/g	305	[37]
5NiS/GR	1 M KOH	1 A/g	774 F/g	This study
10NiS/GR	1 M KOH	1 A/g	724 F/g	This study
15NiS/GR	1 M KOH	1 A/g	510 F/g	This study

the proportion of capacitive and diffusion-controlled contributions can be determined, respectively. The red part represents the capacitive contribution of the 5NiS/GR electrode at different scan rates from 2 to 8 mV/s in Fig. 5b–e. The summary diagram of capacitive contribution as shown in Fig. 5f, some conclusions as obtained: (1) the capacitive contribution is 21.3% at the scan rate of 2 mV/s. (2) with the increase of scan rates, the proportion of capacitive contribution increases, which are 25.8%, 30.9% and 35% at the scan rate of 4, 6 and 8 mV/s, respectively. The smallest capacitive contribution percentage at the lowest scan rate indicates that diffusion-controlled contribution is in charge. The diffusion-controlled contribution occurs in the region of redox peaks, which is directly related to the Faraday reaction rate. It may be because the electrolyte ions have enough time to through the bulk of the electrode material to reach the surface of the electrode material for energy storage when scan rate is low. Therefore, it shows that the 5NiS/GR electrode material is essentially a battery-type material, but it emerges pseudocapacitive behavior after its size reduce [43].

The amount of charge stored at outer surface of the electrode (q_o) and inner surface of the electrode (q_i) can be quantified using Trasatti [44]. The total charge stored (q_T) is a summation of "q_o" and "q_i" as follows [45, 46]:

$$q_T = q_i + q_o \tag{3}$$

where "q_o" is related to the capacitive contribution process, which is not affected by the scan rates [47]. However, "q_i" is associated with the diffusion-controlled contribution process. To show the relationship between the total charge stored and scan rates using the following formula [45, 46].

$$q(v) = q_\infty + kv^{-1/2} \tag{4}$$

where "q" is the amount of charge at various scan rates, "$kv^{-1/2}$" represents the amount of stored charge due to diffusion-controlled contribution ("k" is constant), and "q_∞" represents the charge storage at high scan rate. By drawing the fitting lines of "$v^{1/2}$" vs. "q^{-1}" and "$v^{-1/2}$" vs. "q", the values of "q_T" and "q_o" can be obtained, respectively. When v →0, the value of "q_T" can be calculated by the intercept of the fitting line on the axis ("q_T" = 5459 C/g), as shown in Fig. 5 g. While, from Fig. 5 h, when v → ∞, "q_o" can also be given by the intercept of the fitting line on the axis ("q_o" = 445 C/g). According to formula 4, it shows that the "q_i" of the electrode material is 5014 C/g. Thus, it claims that the energy storage of 5NiS/GR materials is mainly diffusion-controlled contribution.

3 Conclusions

This study reports a novel nickel sulfide composite synthetic strategy that graphene residual carbon (GR) is used for carbon substrate to synthesize NiS/GR composites by hydrothermal method. A series of characterization indicate that 5% content of GR play a significant role in improving electrode electrochemical performance among various GR content (5%, 10%, and 15%). We pointed out three reasons to explain this result. (1) In terms of phase composition, the addition of GR will reduce the crystallinity of NiS. (2) In terms of morphology and structure, the addition of GR will change the microflower-like NiS particles into nanospheres and reduce the particle size, which apt to expose more surface-active site. (3) In terms of electrochemical performance, the 5NiS/GR electrode

(a)

(b)

(c)

(d)

(e)

(f)

(g)

(h)
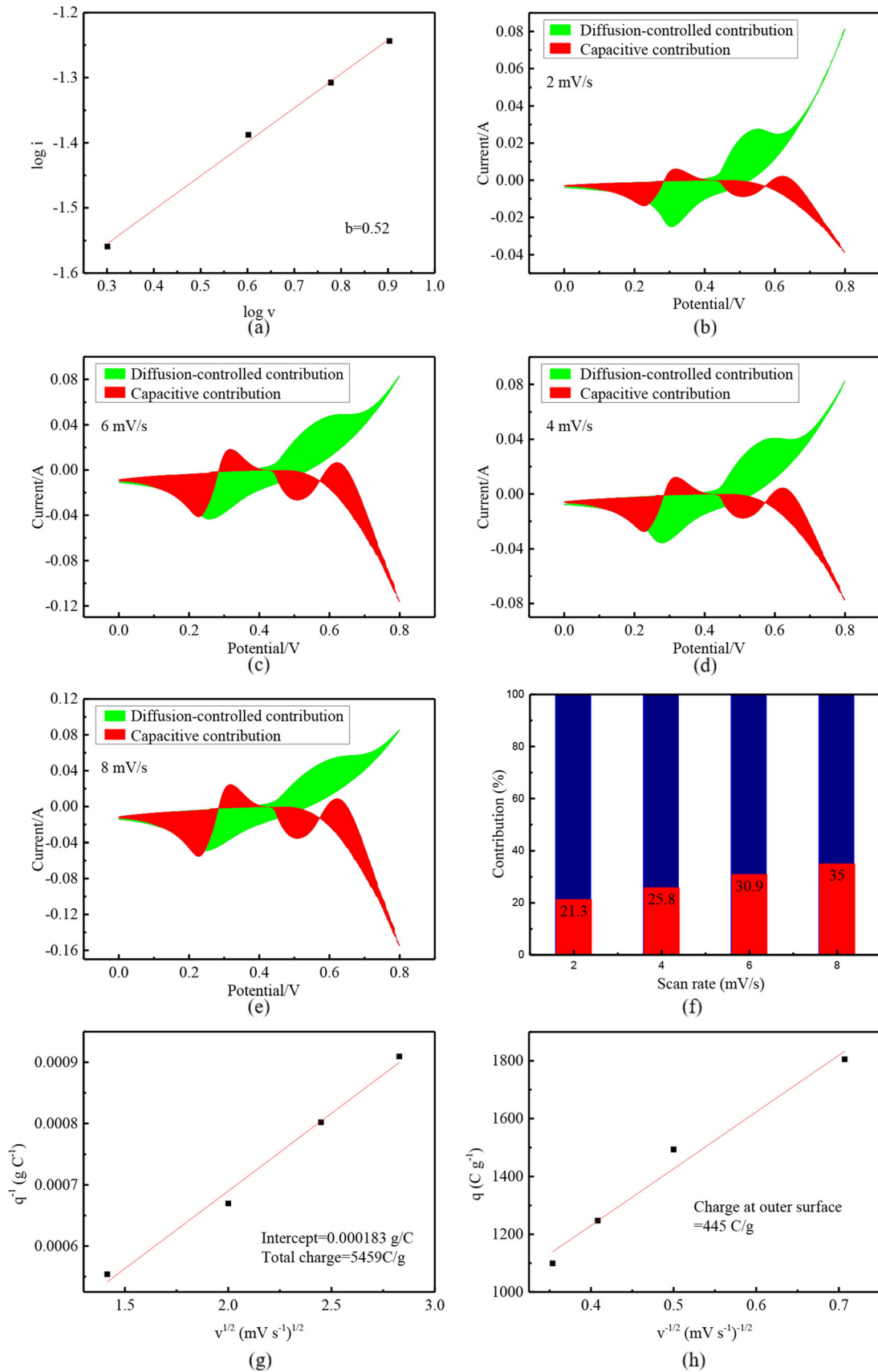
◄ **Fig. 5** **a** log v - log i, **b**–**e** Contribution of surface capacitance to total charge storage at different scanning rates, **f** Comparison of charge storage at different scan rates, **g-h** The relationship between the stored charge and scan rate, **g** v 1/2 vs. q - 1, **h** v - 1/2 vs. q

exhibiting the highest specific capacitance (774 F/g at 1 A/g), good rate capability (78.1% retention after current density increases to 10 A/g) and good cycling performance (77.2% capacitance retention after 1000 cycles at 5 A/g), which indicate that the addition of 5% content GR can immobilize active materials during long-term cycling performance test and improve conductivity of NiS electrode. Through quantitative kinetic analyses, it shows that the energy storage of 5NiS/GR materials is mainly the diffusion-controlled contribution.

4 Methodology section

Main chemicals including graphite powder, nickel acetate, thiourea, and trisodium citrate are used without any further purification.

4.1 Preparation of graphene residual carbon

The synthesis of graphene residual carbon can be is divided into a two-step: carbonization of graphene residue prepared via modified Hummer's method and activation. In the first step, the dried graphene residue was pre-expanded at 170 °C for 30 min. Then, graphene residue is placed in a corundum boat and annealed to 800 °C for an hour in the N_2 atmosphere with a ramping rate of 5 °C/min. The next pathway is too active graphene residue by KOH treatment. The KOH powder and the carbonized graphene residue are dried and mixed in the weight ratio of 3:1. Then, the mixture is placed in a corundum boat then heated to 400 °C at a ramp rate of 5 °C/min and maintained for an hour in the N_2 atmosphere with ramping rate. Next, maintain the boat at 800 °C for an hour. After the whole process, the boat is left to room temperature by cool naturally. Finally, the obtained sample is washed with 3 M HCl and DI water to remove the impurities and dried at 150 °C for 2 h. The final dried product is marked as GR.

4.2 Synthesis of NiS/GR

Three different NiS/GR composites are synthesized as follows: nickel acetate (4 mmol), thiourea, and trisodium citrate in the weight ratio of 1:7:4 are mixed with 50 mL DI water in a glass bottle and magnetic stirring for an hour, followed by addition of GR, which have dissolved in 20 mL deionized water for 4 h. Then magnetic stirring for an hour, again. The mixture is shifted into the autoclave then heated at 200 °C for 12 h. After cooling naturally to room temperature, the precipitate is collected and washed to neutral with DI water, followed by freeze-dried for 48 h. The final composites are obtained and named as 5NiS/GR, 10NiS/GR, and 15NiS/GR, respectively, depending on the weight ratio of GR (5%, 10%, and 15%). To confirm the effect of the addition of GR on the electrochemical performance of NiS, pure NiS is obtained at the same conditions named as NiS.

5 Characterization

5.1 Structural and morphological characterization

The crystalline structure of samples is investigated using X-ray diffraction (XRD-6100) at 40 kV with Cu Kα (λ = 1.54 Å) radiation at 2θ angles from 5° to 80°. The surface morphology of the samples is examined by scanning electron microscope (Hitachi TM3030) and transmission electron microscope (JEOL2100F).

5.2 Electrochemical measurements

Electrochemical characteristics are carried out by CHI660E electrochemical workstation (Chenhua, Shanghai). The working electrode is prepared by mixing 80 wt% of active material (NiS/GR or NiS), 10 wt% of acetylene black, and 10 wt% of polyvinylidene fluoride to form a slurry. The slurry is covered with Ni foam (1 × 1 cm^2) and dried at 60 °C. The electrochemical performance of working electrodes include cyclic voltammetry (CV), galvanostatic charge-discharge (GCD), and electrochemical impedance spectra (EIS, 5 mV amplitude in a frequency range of 1 Hz–100 kHz) are characterized using a traditional three-electrode configuration in 1 M KOH solution. The platinum foil (1 × 1 cm^2) and Hg/HgO electrode were used as the counter and reference

electrodes, respectively. The specific capacitance can be easily calculated by the following equation:

$$C_m = I \times \Delta t / (m \times \Delta V) \tag{5}$$

where C_m, $I(A)$, $\Delta t(s)$, $m(g)$, ΔV represent the specific capacitance (F/g), discharge current (A), discharge time (s), designated mass (g) of the active materials, and voltage change (V), respectively.

Data availability

All data generated or analyzed during this study are included in this published article.

Declarations

Conflict of interest The authors declare that they have no known competing financial interests or personal relationships that could have appeared to influence the work reported in this paper.

References

1. X. Wang, S. Yin, J. Jiang et al., A tightly packed Co_3O_4/C&S composite for high-performance electrochemical supercapacitors from a cobalt(III) cluster-based coordination precursor. J. Solid State Chem. **288**, 121435 (2020)
2. D.P. Dubal, O. Ayyad, V. Ruiz et al., Hybrid energy storage: the merging of battery and supercapacitor chemistries. Chem. Soc. Rev. **44**(7), 1777–1790 (2015)
3. H. Wei, D. Cui, J. Ma et al., Energy conversion technologies towards self-powered electrochemical energy storage systems: the state of the art and perspectives. J. Mater. Chem. A **5**(5), 1873–1894 (2017)
4. H. Niu, X. Yang, Q. Wang et al., Electrostatic self-assembly of MXene and edge-rich CoAl layered double hydroxide on molecular-scale with superhigh volumetric performances. J. Energy Chem. **46**, 105–113 (2020)
5. K. Li, X. Liu, T. Zheng et al., Tuning MnO_2 to FeOOH replicas with bio-template 3D morphology as electrodes for high performance asymmetric supercapacitors. Chem. Eng. J. **370**, 136–147 (2019)
6. L. Lai, M. Clark, S. Su et al., Dip-coating synthesis of rGO/α-Ni(OH)@nickel foam with layer-by-layer structure for high performance binder-free supercapacitors. Mater. Sci. **368**, 137589–137622 (2021)
7. T. Wang, K. Li, Q. Le et al., Tuning parallel manganese dioxide to hollow parallel hydroxyl oxidize iron replicas for high-performance asymmetric supercapacitors. J. Colloid Interface Sci. **594**, 812–823 (2021)
8. A. Mohanty, D. Jaihindh, Y.-P. Fu et al., An extensive review on three dimension architectural metal-organic frameworks towards supercapacitor application. J. Power Sources **488**, 229444 (2021)
9. K. Li, S. Feng, C. Jing et al., Assembling a double shell on a diatomite skeleton ternary complex with conductive polypyrrole for the enhancement of supercapacitors. Chem. Commun. **55**(91), 13773–13776 (2019)
10. A. Borenstein, O. Hanna, R. Attias et al., Carbon-based composite materials for supercapacitor electrodes: a review. J. Mater. Chem. A **5**(25), 12653–12672 (2017)
11. K.-B. Wang, Q. Xun, Q. Zhang, Recent progress in metal-organic frameworks as active materials for supercapacitors. EnergyChem **2**(1), 100025 (2020)
12. S.-C. Wang, D. Xiong, C. Chen et al., The controlled fabrication of hierarchical CoS_2@NiS_2 core-shell nanocubes by utilizing prussian blue analogue for enhanced capacitive energy storage performance. J. Power Sources **450**, 227712–227723 (2020)
13. J. Xu, L. Zhang, G. Xu et al., Facile synthesis of NiS anchored carbon nanofibers for high-performance supercapacitors. Appl. Surf. Sci. **434**, 112–119 (2018)
14. D. Jiang, H. Liang, W. Yang et al., Screen-printable films of graphene/CoS_2/Ni_3S_4 composites for the fabrication of flexible and arbitrary-shaped all-solid-state hybrid supercapacitors. Carbon **146**, 557–567 (2019)
15. M. Govindasamy, S. Shanthi, E. Elaiyappillai et al., Fabrication of hierarchical $NiCo_2S_4$@CoS_2 nanostructures on highly conductive flexible carbon cloth substrate as a hybrid electrode material for supercapacitors with enhanced electrochemical performance. Electrochim. Acta **293**, 328–337 (2019)
16. J. Zhao, B. Guan, B. Hu et al., Vulcanizing time controlled synthesis of NiS microflowers and its application in asymmetric supercapacitors. Electrochim. Acta **230**, 428–437 (2017)
17. Q. Hu, X. Zou, Y. Huang et al., Graphene oxide-drove transformation of NiS/Ni_3S_4 microbars towards Ni_3S_4

polyhedrons for supercapacitor. J. Colloid Interface Sci. **559**, 115–123 (2020)

18. Q. Hu, W. Li, B. Xiang et al., Sulfur source-inspired synthesis of β-NiS with high specific capacity and tunable morphologies for hybrid supercapacitor. Electrochim. Acta **337**, 135826–135836 (2020)

19. A. Bazan-Aguilar, M. Ponce-Vargas, C.L. Caycho et al., Highly porous reduced graphene oxide-coated carbonized cotton fibers as supercapacitor electrodes. ACS Omega **5**(50), 32149–32159 (2020)

20. J. Zhang, D. Zhang, B. Yang et al., Targeted synthesis of NiS and NiS_2 nanoparticles for high–performance hybrid supercapacitor via a facile green solid–phase synthesis route. J. Energy Storage **32**, 101852–101861 (2020)

21. J. Wu, F. Wei, Y. Sui et al., Interconnected NiS-nanosheets@porous carbon derived from Zeolitic-imidazolate frameworks (ZIFs) as electrode materials for high-performance hybrid supercapacitors. Int. J. Hydrogen Energy **45**(38), 19237–19245 (2020)

22. H. Xie, J. Li, C. Chen et al., Preparation and supercapacitor performance of $NiO/CuO_{-0.3}/GO_{-30}$ nanoplates. Mater. Lett. **282**, 128887–128890 (2021)

23. X. Zhang, Q. Lu, H. Liu et al., Nature-inspired design of NiS/carbon microspheres for high-performance hybrid supercapacitors. Appl. Surf. Sci. **528**, 146976 (2020)

24. Y. Zheng, Y. Tian, S. Sarwar et al., Carbon nanotubes decorated $NiSe_2$ nanosheets for high-performance supercapacitors. J. Power Sources **452**, 227793–227800 (2020)

25. W. Niu, Z. Xiao, S. Wang et al., Synthesis of nickel sulfide-supported on porous carbon from a natural seaweed-derived polysaccharide for high-performance supercapacitors. J. Alloy. Compd. **853**, 157123 (2021)

26. N. Chakrabarty, A.K. Chakraborty, Controlling the electrochemical performance of β-$Ni(OH)_2$/carbon nanotube hybrid electrodes for supercapacitor applications by La doping: a systematic investigation. Electrochim. Acta **297**, 173–187 (2019)

27. S. Harish, A.N. Naveen, R. Abinaya et al., Enhanced performance on capacity retention of hierarchical NiS hexagonal nanoplate for highly stable asymmetric supercapacitor. Electrochim. Acta **283**, 1053–1062 (2018)

28. S. Ma, S. Zhou, S. Wang et al., Controlled synthesis of $Ni_{0.85}Se$ microstructures with different morphologies and their morphology-dependent electrochemical supercapacitor properties. J. Alloy. Compd. **728**, 592–599 (2017)

29. M. Manuraj, K.V. Kavya Nair, K.N.N. Unni et al., High performance supercapacitors based on MoS_2 nanostructures with near commercial mass loading. J. Alloy. Compd. **819**, 152963–152988 (2020)

30. T. Zhai, S. Sun, X. Liu et al., Achieving insertion-like capacity at ultrahigh rate via tunable surface pseudocapacitance. Adv Mater **30**(12), e1706640 (2018)

31. S.S. Rao, D. Punnoose, J.-H. Bae et al., Preparation and electrochemical performances of NiS with PEDOT:PSS chrysanthemum petal like nanostructure for high performance supercapacitors. Electrochim. Acta **254**, 269–279 (2017)

32. S.-Y. Kim, C.V.V.M. Gopi, A.E. Reddy et al., Facile synthesis of a NiO/NiS hybrid and its use as an efficient electrode material for supercapacitor applications. New J. Chem. **42**(7), 5309–5313 (2018)

33. X. Yue, R. Hu, D. Zhu et al., Controlled synthesis and formation mechanism of flower-like CuS/NiS microspheres for supercapacitors. Surf. Interfaces **22**, 100871 (2021)

34. S. Sahoo, A.K. Satpati, P.K. Sahoo et al., Incorporation of carbon quantum dots for improvement of supercapacitor performance of nickel sulfide. ACS Omega **3**(12), 17936–17946 (2018)

35. Y. Zheng, Y. Tian, S. Liu et al., One-step microwave synthesis of NiO/NiS@CNT nanocomposites for high-cycling-stability supercapacitors. J. Alloy. Compd. **806**, 170–179 (2019)

36. J. Yang, X. Duan, W. Guo et al., Electrochemical performances investigation of NiS/rGO composite as electrode material for supercapacitors. Nano Energy **5**, 74–81 (2014)

37. N.A. Marand, S.M. Masoudpanah, S. Alamolhoda et al., Solution combustion synthesis of nickel sulfide/reduced graphene oxide composite powders as electrode materials for high-performance supercapacitors. J. Energy Storage **39**, 102637 (2021)

38. M.M. Baig, I.H. Gul, M.Z. Khan et al., Binder-free heterostructured MWCNTs/AlS decorated on NiCo foam as highly reversible cathode material for high-performance supercapacitors. Mater. Sci. **340**(2020)

39. Q. Zong, H. Yang, Q. Wang et al., Three-dimensional coral-like $NiCoP@C@Ni(OH)_2$ core-shell nanoarrays as battery-type electrodes to enhance cycle stability and energy density for hybrid supercapacitors. Chem. Eng. J. **361**, 1–11 (2019)

40. Y. Lu, J. Liang, Y. Hu et al., Accurate control multiple active sites of carbonaceous anode for high performance sodium storage: insights into capacitive contribution mechanism. Adv. Energy Mater. **10**(7), 1903312 (2020)

41. C. Liu, X. Wu, B. Wang, Performance modulation of energy storage devices: a case of Ni-Co-S electrode materials. Chem. Eng. J. **392**, 123651 (2020)

42. V. Augustyn, P. Simon, B. Dunn, Pseudocapacitive oxide materials for high-rate electrochemical energy storage. Energy Environ. Sci. **7**(5), 1597–1614 (2014)

43. Y. Jiang, J. Liu, Definitions of pseudocapacitive materials: a brief review. Energy Environ. Mater. **2**(1), 30–37 (2019)

44. V. Boychuk, V. Kotsyubynsky, B. Rachiy et al., β-Ni(OH)/ reduced graphene oxide composite as electrode for supercapacitors. Mater. Today **6**, 106–115 (2019)

45. J. Yan, C.E. Ren, K. Maleski et al., Flexible MXene/graphene films for ultrafast supercapacitors with outstanding volumetric capacitance. Adv. Func. Mater. **27**(30), 1701264 (2017)

46. H. Niu, Z. Zou, Q. Wang et al., Structurally stable ultrathin 1T-2H MoS$_2$ heterostructures coaxially aligned on carbon nanofibers toward superhigh-energy-density supercapacitor

and enhanced electrocatalysis. Chem. Eng. J. **399**, 125672 (2020)

47. Y.H. Lee, K.H. Chang, C.C. Hu, Differentiate the pseudocapacitance and double-layer capacitance contributions for nitrogen-doped reduced graphene oxide in acidic and alkaline electrolytes. J. Power Sources **227**, 300–308 (2013)